Journal Pre-proofs

Simulation-assisted hapten screening for sensitive on-site and visual detection of diazinon pesticide in environmental water and food samples

Xiaoling Li, Aihong Wu, Maozhong Sun, Shanshan Song, Hua Kuang, Chuanlai Xu, Xiaoling Wu

PII: S1385-8947(24)10508-6
DOI: https://doi.org/10.1016/j.cej.2024.159017
Reference: CEJ 159017

To appear in: *Chemical Engineering Journal*

Received Date: 26 September 2024
Revised Date: 2 December 2024
Accepted Date: 26 December 2024

Please cite this article as: X. Li, A. Wu, M. Sun, S. Song, H. Kuang, C. Xu, X. Wu, Simulation-assisted hapten screening for sensitive on-site and visual detection of diazinon pesticide in environmental water and food samples, *Chemical Engineering Journal* (2024), doi: https://doi.org/10.1016/j.cej.2024.159017

Simulation-assisted hapten screening for sensitive on-site and visual detection of diazinon pesticide in environmental water and food samples

Xiaoling Li[1,2,3], Aihong Wu[1,2,3], Maozhong Sun[1,2,3], Shanshan Song[1,2,3], Hua Kuang[1,2,3], Chuanlai Xu[1,2,3], Xiaoling Wu[1,2,3*]

[1] *Food Science and Technology, Jiangnan University, Wuxi, Jiangsu, 214122, People's Republic of China;*

[2]*International Joint Research Laboratory for Biointerface and Biodetection, and School of* [3]*Collaborative Innovation Center of Food Safety and Quality Control in Jiangsu Province, Jiangnan University, Wuxi, Jiangsu, 214122, People's Republic of China;*[4]*Jiangsu Product Quality Testing and Inspection Institute，Nanjing, Jiangsu,210000, China*

[*]Corresponding author, Email: wuxiaoling@jiangnan.edu.cn

One Sentence Summary: An on-site and visual strip for rapid Diazinon detection

ABSTRACT

Diazinon (DAZ) is an important organophosphorus pesticide, widely retained in the environmental and food samples, badly affecting the ecological environment and human health. The rapid screening and accurate quantitative detection of DAZ are of great significance for environmental and food safety. This study proposed a novel hapten and evaluated its design rationale based on computer simulation analysis of molecular structural similarity, matching degree, and energetic state. Then, a sensitive monoclonal antibody (mAb) was successfully prepared, with a semi-inhibitory concentration (IC_{50}) of 0.4 ng/mL for DAZ in an indirect competitive enzyme-linked immunosorbent assay (ic-ELISA). We analyzed the relationship between the similarity of haptens and antibody performance, providing new possibilities and methods for developing antibodies against other small molecule compounds. Moreover, we successfully developed colloidal gold immunochromatographic assay (CG-ICA) strips for on-site and visual detection of DAZ in water and food samples, and visual limit of detection (v-LOD) was 0.2 μg/L in lake water, and 0.5 μg/kg in vegetables. The recovery rates were 87.35–106.20% and coefficients of variation were 1.37–7.60%. And the accuracy of the method was further demonstrated by the liquid chromatography–tandem mass spectrometry method. This study is a new exploration in the DAZ detection method, providing ideas for rapid screening and accurate quantitative analysis of typical and new environmental pollutants.

KEYWORDS: diazinon pesticide; on-site and visual detection; colloidal gold immunochromatographic assay (CG-ICA) strip; environmental pollutants; computer simulation analysis

1. Introduction

Diazinon (DAZ), a broad-spectrum and highly effective organophosphorus pesticide, is commonly applied to crops such as rice, tree fruits, and vegetables. However, its widespread use has also resulted in significant environmental pollution and health risk. The detected residue range of DAZ pesticide in fruits and vegetables from Argentina, Bangladesh, and South Korea from 2015 to 2020 was about 20–451.4 μg/kg. Most of the DAZ was distributed in the environment, with a residue range of 0.44–7.29 μg/kg in soil of Baiyangdian Lake in 2020, and 0.02–2100 μg/L in water of Guangzhou in 2017 and Sefidroud River in 2015 [1-4]. It may leave behind residues that are harmful to environmental and human health through water and food chains, potentially causing neurological and endocrine damage [1, 5-11]. To ensure food safety, maximum residue levels (MRLs) for DAZ have been established, with ranges from 0.01 to 5 mg/kg in China (national food safety standard (GB2763-2021) in China) and the European Union [12]. Consequently, efficient and accurate detection methods for DAZ are vital for safeguarding environmental and food safety.

Although traditional gas chromatography–mass spectrometry [13] and high-performance liquid chromatography [14] methods for detecting DAZ are sensitive and accurate, their competitiveness in rapid testing is limited due to the special requirements for equipment installation and the time-consuming nature of the tests. Visual test strips, as a paper-based point of care (POC) rapid detection strategy, are utilized for the swift identification of pesticide residues [15-17]. In contrast, immunoassay methods, particularly lateral flow immunoassay, offer high specificity and are suitable for on-site rapid detection, making them widely employed in food contamination monitoring and various other fields [18], with colloidal gold immunochromatographic assay (CG-ICA) being the most extensively applied. So far, we have not found the application of rapid on-site visual detection strips for DAZ in previous reports. We aim to develop a low-cost, high-throughput, and visually verifiable CG-ICA test strip using the highly affinity and highly sensitivity anti-DAZ antibodies.

The development of efficient CG-ICA relies on high-performance antibodies, where the differences in antibody performance are primarily caused by the heterogeneity of hapten structures [19, 20]. Various hapten design strategies lead to different functional outcomes of the resulting antibodies. The structure of DAZ consists of a pyrazine ring and a phosphorothioate group; Previous studies have reported that haptens prepared by modifying either of these two groups induced anti-DAZ antibodies, but the cross-reactivity with analogs such as pirimiphos-ethyl (PMP-E), chlorpyrifos (CPF), diazoxon (DAX), and triazophos (TZP) was less than 5% [21, 22]. All these analogs contain a pyrazine ring or a phosphorothioate group, with PMP-E having a structure similar to DAZ, including both a pyrazine ring and an ethyl phosphorothioate group, yet the literature does not provide an explanation for this phenomenon. The influence of hapten structure on the functionality of anti-DAZ antibodies is still a matter of uncertainty. Computer simulation analysis plays a significant role in the preparation of high-performance antibodies; in particular, the similarity between hapten and the target molecule in the simulation analysis is crucial for generating highly sensitive antibodies [20].

In this research, we introduced a novel hapten that allowed the positioning of the linker arm to expose the phosphorothioate group after conjugation to carrier proteins, suggesting the potential to generate antibodies with multiple cross-reactivities. We conducted computer simulation analysis to assess the similarity and matching of molecular structures, and employed molecular modeling to assist in enhancing antibody sensitivity and explaining antibody cross-reactivity, followed by experimental validation. The aim of this study is to utilize computer simulation analysis to evaluate the structural similarity between different haptens and DAZ, and to select haptens with similar molecular structures and energy distributions. Furthermore, the mAbs prepared were applied in the development of CG-ICA strips for rapid detection of DAZ in actual samples. The proposed CG-ICA offers advantages of speed, simplicity, cost-effectiveness, and on-site detection, making it a promising tool for ensuring food safety and security in the context of DAZ residue monitoring.

2. Materials and methods

2.1.Chemicals and materials

We obtained keyhole limpet hemocyanin (KLH, ≥98%), N,N-dimethylformamide (DMF), bovine serum albumin (BSA, ≥98%), dimethyl sulfoxide (DMSO), Freund's adjuvant, 1-ethyl-carbodiimidehydrochloride (EDC, ≥98%), N-hydroxysuccinimide (NHS, ≥98%), ethyl 4-cyanobutanoate (≥98%), ethyl 3-oxobutanoate (≥98%), DAZ (≥98%), CPF (≥98%), chlorpyrifos-methyl (CPF-M, ≥98%), PMP-E (≥98%), pirimiphos-methyl (PMP-M, 97.5%), TZP (≥98%), DAX (≥98%) from J&K Scientific Ltd. (Shanghai, China). We obtained horseradish peroxidase (HRP)-labeled goat anti-mouse IgG antibody and goat anti-mouse IgG antibody from Jackson ImmunoResearch Laboratories, Inc. (West Grove, PA, USA). We purchased a commercial ELISA kit from Biodragon Technology Co., Ltd. (Suzhou, China). We purchased the nitrocellulose (NC) high-flow membranes (Pura-bind RHATF 10050) from Whatman-Xinhua Filter Paper Co., Ltd. (Hangzhou, China). The absorbent pad, polyvinylchloride (PVC) backing material, and glass fiber membrane were obtained from Jiasheng Plastic Packaging Products Co., Ltd. (Dongguan, China). We purchased a digital colloidal gold reader from Wuxi Determine Bio-Tech Co., Ltd. (Wuxi, China).

2.2.Computer simulation analysis of Haptens

Starting from the structure of DAZ itself, we designed a new hapten (DAZ-hapten) by deriving carboxyl groups on pyrimidine rings to expose the organophosphorus group, and utilized a computer simulation analysis to predict the rationality of the hapten. We conducted a structural assessment of DAZ's structure, analogs, and the hapten using the ChemBioOffice software (PerkinElmer, Waltham, MA, USA) and the Gaussian software package (Gaussian, Wallingford, CT, USA). By analyzing their chemical structural characteristics, including structural similarity, lowest-energy conformations, atomic charge distribution, and molecular electrostatic potential distribution, we derived the DAZ-hapten based on the most feasible outcomes. The lowest energy states of various molecules were optimized using the MM2 force field in ChemBio3D Ultra 14.0 software, and the surface charge distribution was calculated using Gaussian 09 to

determine Mulliken charges. The lowest-energy conformations were calculated and optimized using density functional theory (DFT) with the B3LYP functional and the 6-31G* basis set in Gaussian software, and the molecular electrostatic potential maps were visualized using Multiwfn and VMD. In addition, we invoked RDKit within a Python program to calculate the similarity of characteristic groups between chemical residues and the hapten. Finally, we selected hapten candidates with highly-similar structures and surface charge distributions to the analyte, based on the desired properties of the target antibody, for derivative synthesis.

2.3.Synthesis of Hapten and Complete Antigens

2.3.1 Synthesis of hapten

The DAZ-hapten was obtained through de novo synthesis. Final product, the DAZ-hapten, was identified using liquid chromatography–tandem mass spectrometry (LC–MS) and nuclear magnetic resonance spectroscopy (^{1}H NMR). The specific instruments and testing conditions are provided in **Table S2** of the **Supporting Information**.

2.3.2 Preparation of complete antigen

The DAZ-hapten, confirmed as successfully obtained by nuclear magnetic resonance spectroscopy and mass spectrometry, was coupled to carrier proteins (KLH and BSA). The conjugation process employed the active ester method [23], and the procedure was as follows:

We dissolved 6.2 mg of DAZ-hapten in DMF and stirred the solution at room temperature. We then added 6.2 mg of NHS, followed by the addition of 10.2 mg of EDC after a 15-minute interval. After 4 h of reaction, we evenly divided this solution between 10 mg KLH or BSA, pre-dissolved in borate buffer solution (BBS, containing boric acid and sodium hydroxide) to a concentration of 4 mg/mL. Following an overnight stirring reaction (approximately 12 h) and dialysis, we obtained the immunizing antigen DAZ-hapten-KLH and the coating antigen DAZ-hapten-BSA. The conjugates were characterized by ultraviolet–visible spectrophotometry (UV–Vis) and stored at 4°C in a refrigerator for future use.

2.4. Preparation and identification of the mAb

2.4.1 Preparation of the mAb

We successfully immunized ten mice with immunizations (DAZ-hapten-KLH) given at regular intervals. A dose of 100 μg per mouse was used for the BALB/c mice; four weeks later, a booster immunization was given with 50 μg per mouse. Subsequently, we conducted a booster immunization every three weeks. One week following the fifth immunization, blood was collected from the tails of the mice and tested. The coating antigen DAZ-hapten-BSA was diluted in a three-fold gradient from 0.3 μg/mL to four concentrations for testing the titer of mouse serum and assessing its inhibition on DAZ standard. The titers and inhibition at a DAZ standard concentration of 5 ng/mL were measured. The titer was defined as the antiserum dilution at which the antigen was diluted to 1/30,000 and the OD_{450nm}-max fell between 1.4 and 2.0 [24]. The calculation formula for inhibition was (1):

$$\text{Inhibition } (\%) = 1 - \frac{B}{B0} * 100\% \quad (1).$$

In the formula, B0 represents the OD_{450nm} value of the control wells without the addition of standards, while B is the OD_{450nm} value of the experimental wells with standards added.

Mice with both a good serum titer and good inhibition were selected for cell fusion. We harvested a mouse spleen and finely ground them through a 200-mesh sterile sieve to obtain spleen cells. These spleen cells were then mixed with SP2/0 cells and fused using polyethylene glycol (PEG) 1450. After fusion, the cells were cultured in a 96 microporous plate and subjected to four rounds of subcloning of cell well screening and cultivation, resulting in the isolation of a single antibody-secreting cell line. Following expansion and culture, the cell line produced ascites, which was then purified to obtain the mAb.

2.4.2 Performance of the mAb

2.4.2.1 Isotype and Affinity

The coating antigen concentration was set to 0.3 μg/mL and immobilized on the microplate, followed by the detection of the mAb using a mouse monoclonal antibody subtype identification kit (ELISA kit).

The binding affinity between antibodies and antigenic determinants is termed antibody affinity, which is quantified by the equilibrium constant K_a [25]. The ic-ELISA method can meet the general requirements for antibody affinity measurement. The antigen was coated onto the plate in a gradient concentration with three replicates. The mAb was diluted in a three-fold gradient starting from 1 μg/mL down to eight concentrations, and an S-shaped fitting curve was established. The log value of the antibody concentration was used as the X-axis, and the corresponding absorbance at 450 nm was used as the Y-axis [25]. The formula was given by equation (2):

$$K_a = \frac{n-1}{2*n*[Ab']_t - [Ab]_t} \quad (2).$$

In the formula, n represents the ratio of the concentrations of the two antigen groups; $[Ab]_t$ represents the antibody concentration (mol/L) corresponding to half of the maximum signal at a certain antigen concentration. A higher K_a value indicates a stronger selective binding ability of the antibody to the target antigen, with less cross-reaction with non-target molecules, resulting in better accuracy of the detection.

2.4.2.2 Optimization and establishment of a fitting curve

To better assess the performance of the obtained mAb, we optimized the conditions in the ELISA. A solution of 0.01 M PBS(K^+) (containing potassium dihydrogen phosphate, potassium chloride, sodium chloride, and dipotassium dihydrogen phosphate) with a pH of 7.4 was selected as the basic solution, and organic solvents such as ethanol (EtOH), methanol (MeOH), DMF, DMSO, and acetonitrile (ACN) were individually added to the 0.01 M PBS (K^+) [26]. The solvent effect patterns

of different buffer systems on the mAb were investigated, as well as the tolerance of the mAb to various organic solvents.

Under the above optimization conditions, we established an S-shaped fitting curve for mAb. The log values of DAZ standard concentrations (0, 0.021, 0.062, 0.18, 0.56, 1.67, 5, and 15 ng/mL) were used as the X-axis, and the absorbance values at a detection wavelength of 450 nm were used as the Y-axis. After processing with Oringin software, a fitting curve of the mAb was obtained.

2.4.2.3 Cross-reactivity

Using the same detection procedure, the mAb was used to detect the inhibition of DAX, CPF, CPF-M, PMP-E, PMP-M, TZP, quinalphos (QNP), parathion (PTN), phoxim, parathion-methyl (PTN-M), fenitrothion (FNT), and etrimfos. The cross-reactivity rate was calculated using formula (3):

$$\text{Cross} - \text{reactivity rate}(\%) = \frac{\text{IC}_{50}\text{ value of DAZ}}{\text{IC}_{50}\text{ value of other analytes}} * 100\% \quad (3).$$

2.5. Preparation of colloidal gold-labeled mAb conjugates and the CG-ICA strip

2.5.1 Mab modification of colloidal gold

The synthesis of colloidal gold (15 nm) and colloidal gold-labeled mAb conjugates followed the method described in a previous study with slight modifications. Initially, the mAb was added to a 10 mL solution of colloidal gold that had been previously adjusted to a pH of approximately 8.2 with 0.02 M K_2CO_3 solution. After gentle stirring, the reaction was allowed to stand for 1 hour. Then, 10% (m/v) BSA was added and the mixture was incubated for 2 h to block further binding reactions of the complexes. After the labeling was complete, the mixture was centrifuged at 8500 r/mim for 50-minute to remove the unbound mAb protein and excess colloidal gold. Finally, the pellet was resuspended in 0.01 M PBS(K^+) containing mannitol, sucrose, sorbitol, trehalose, and Tween-20 to obtain stable colloidal gold-labeled mAb conjugates [27].

2.5.2 Assembly of the CG-ICA strip

The test strip's substrate material functions as the supporting structure and contains four fixed areas: the sample pad, conjugate pad, nitrocellulose (NC) membrane, and absorbent pad. The NC membrane is the core component of the test strip. On the NC membrane, a control line (C-line) is pre-fixed with goat anti-mouse IgG antibody to verify the functionality of the test strip, and a test line (T-line) coated with antigen is pre-fixed to capture the colloidal gold-labeled mAb conjugates. The conjugate pad, which connects to the NC membrane and the sample pad, is coated with the colloidal gold-labeled mAb conjugates. The NC membrane is positioned with the conjugate pad in front and the absorbent pad behind. Once cut to size, the entire test strip is inserted into the casing, allowing the C- and T-lines to be visible through the display window [28].

2.5.3 Operating principle of the CG-ICA strip

The sample to be tested was applied onto the sample pad, where it would subsequently pass through the conjugate pad and the NC membrane via capillary action. The sample solution carried away the colloidal gold-labeled mAb conjugates from the conjugate pad and was intercepted by the NC membrane. If the sample solution contained the target, it would first occupy the binding sites on the mAb, resulting in the solution missing the antigen on the T-line and predominantly binding with the goat anti-mouse IgG antibody on the C-line as it flowed through the NC membrane. If the sample did not contain the target, the mAb would be intercepted by the antigen on the T-line, with the remainder binding to the goat anti-mouse IgG antibody on the C-line. The accumulation of colloidal gold-labeled mAb conjugates at specific positions results in the formation of visible red lines. A faint color development on the T-line indicates a positive sample [29].

2.5.4 Optimization of CG-ICA strip detection

In the preparation of colloidal gold-labeled mAb conjugates, the optimal amount of antibody labeled will produce clear and easily readable signals. Meanwhile, the amount of K_2CO_3 used to adjust pH is crucial for achieving optimal labeling results. Following labeling, selecting an appropriate resuspension can maintain the activity of the mAb, ensure the stability of the mAb and detection signal, and promote efficient and stable mAb to colloidal gold binding during testing. The concentration of antigens directly affects the sensitivity of detection on the NC membrane. Therefore, we optimized the antigen concentration, the amount of mAb and K_2CO_3, and resuspension solution when preparing the CG-ICA strips [30]. We also evaluated the T/C value and inhibition rate (IR) after adding the standard using the colloidal gold reader. The formula for calculating inhibition rate was (4):

$$\text{IR}\ (\%) = \left(1 - \frac{\text{T}}{\text{T0}}\right) \times 100\% \quad (4).$$

In the formula, T0 and T represent the T/C values at 0 μg/kg and 10 μg/kg DAZ standard, respectively. Thus, a standard curve for the CG-ICA test strip was established in 0.01M PBS(K^+).

2.6. Sample testing of CG-ICA test strips

2.6.1 Pretreatment of samples

Water samples were collected from a local lake, while food samples were purchased from markets in Wuxi. The lake water did not require treatment; it was directly tested using CG-ICA strips. The edible parts of the food samples (radish, cucumber, strawberry) were cut into small pieces. We added 10 mL of extraction solution to the 5 g sample before homogenization. After homogenization, we added the supernatant solution to the test buffer solution and tested it in triplicate using the recommended CG-ICA strips. Different extraction solvents, dilutions, and diluent solutions were compared for detection results. For LC–MS analysis, the lake water was filtered through a 0.22 μm membrane and pretreatment for food samples was carried out in accordance with the China National Food Standards GB 23200.12-2021.

2.6.2 Testing of CG-ICA strips in fruit and vegetable samples

DAZ standard samples (0, 0.2, 0.5, 1, 2, 5, and 10 μg/L in lake water samples, 0, 0.5, 1, 2, 5, 10, and 20 μg/kg in radish samples, and 0, 1, 2, 5, 10, 20, and 50 μg/kg in cucumber and strawberry samples) were tested using CG-ICA test strips to generate standard curves and scanned using the colloidal gold reader. In addition, 20 confirmed negative samples were tested using CG-ICA test strips [26]. The sensitivity calculation formulas for CG-ICA were (5) and (6) [31]:

$$\text{Limit of detection (LOD)} = \text{Blank} \pm 3 * \text{standard deviation(SD)} \quad (5);$$

$$\text{Limit of quantitation (LOQ)} = \text{Blank} \pm 10 * \text{SD} \quad (6).$$

2.6.3 Recovery experiment

The DAZ standards were prepared at concentrations of 1 and 5 μg/L in lake water and radish samples, as well as 2 and 15 μg/kg in cucumber and strawberry samples. After the above pre-treatment, the prepared test strip was used for three parallel tests. The formula for the rate of recovery was (7):

$$\text{Recovery (\%)} = \left(\frac{\text{Detected value}}{\text{spiked value}}\right) * 100\% \quad (7).$$

2.6.4 Stability analysis

To evaluate the durability of the test strips, an accelerated stability test was carried out by maintaining the test strips in a drying oven at 37°C. Samples of water and radish (containing 1 and 5 μg/L (μg/kg) of DAZ) were tested in triplicate at 0, 7, 14, and 28 days. The obtained T/C values indicated the changes in the test strips [32, 33].

2.7. Sample testing

The CG-ICA detection results of water and food samples were validated by LC–MS following the proposed pretreatment.

3. Results and discussion

3.1.Computer simulation analysis and hapten selection

The structure of the hapten significantly influences the performance of the induced antibodies, which is crucial for enhancing the sensitivity and specificity of detection [20]. The high sensitivity of antibodies for the target molecule is key to solving detection issues [18]; The degree of structural similarity between the hapten and the target molecule is an important factor in producing antibodies with high sensitivity [34]. By predicting the structural similarity and three-dimensional correlation between the hapten and the target molecule, the hapten can be rationally designed to influence the performance of the induced antibodies [35].

Reportedly, the haptens for DAZ (as shown in **Fig. 1b**) could induce antibodies with good selectivity for the single target molecule [21, 22]. Both haptens 2 and 3 exposed the pyrimidine ring of DAZ, thus the prepared antibodies have high specificity

for DAZ with less cross-reactivity with other substances. Despite the introduction of a linker arm at the C10 atom of hapten 1, exposing the phosphorothioate group, its cross-reactivity with other compounds containing this group remained less than 5%. Observing the structures of analogues, it is not difficult to find that the structural difference between DAZ and PMP-E mainly lies in the branched chain at the C10 atom, and they share the same phosphorothioate (ethyl) target group with CPF and the pyrazine ring with DAX (structures shown in **Fig. 1a**). We explored whether the branched chain causes differences in antibody affinity and designed a new DAZ-hapten structure similar to hapten 1, introducing a linker arm at the C10 atom and exposing the phosphorothioate group, aiming to break the cross-reactivity of similar target groups, i.e., by changing the position and shape of the linker arm to enhance group specificity.

The similarity of the four immunological haptens with the four aforementioned similar substances is shown in **Fig. 1c**, where hapten 1 and DAZ-hapten have better uniformity in similarity, and DAZ-hapten has a higher similarity to DAZ. The complete similarity between different haptens and other analogs is presented in **Table S1**. By simulating the molecular lowest energy states of DAZ with different haptens, their molecular spatial structures were observed and compared. After optimization with the MM2 force field, the molecular spatial structure of DAZ and the DAZ-hapten overlapped well, while other haptens had varying degrees of angular twist with DAZ (as shown in **Fig. 1d**). When both hapten 1 and DAZ-hapten introduced linker arms at the C10 atom, a shift was observed in the alignment of hapten 1 with DAZ in three-dimensional structure. This shift may be due to the presence of the "S" atom in the introduced linker arm or the length of the chain, causing changes in the lowest energy state of its spatial structure. Therefore, the design of DAZ-hapten was reasonable at the molecular structure level. After introducing the linker arm, the change in atomic charge distribution at the C10 and C16 atoms is less than 0.2 a.u., and it did not cause significant changes in the spatial conformation of DAZ-hapten and DAZ (as shown in **Fig. 1e** and **1f**), which supports the intuitive model of the molecule and lays the foundation for further hapten synthesis and mouse immunization experiments.

3.2. Characterization of hapten and complete antigens

The synthetic route of the hapten synthesized *de novo* is shown in **Fig. 2a**. The hapten was verified by liquid chromatography, mass spectrometry, and nuclear magnetic resonance spectroscopy (**Fig. 2c, 2d,** and **2e**). The molecular weight of the hapten was 348, with a retention time of approximately 1.22 on the chromatographic column, and a $[M+H]^+$ of 349 in the positive ion mode. This confirmed the successful *de novo* synthesis of the hapten. Liquid phase detection at 254 nm yielded an integrated peak area for the target compound of 99.36%, indicating high purity and supporting subsequent experiments.

After the hapten was coupled with the carrier protein (**Fig. 2b)**, the complete antigen was scanned and the results were shown in **Fig. S2**. Both KLH and BSA showed peaks around 280, while the hapten peaked around 300. The conjugate exhibited a superimposition of the peak shapes of the carrier protein and the hapten, with a red shift observed. This demonstrated that the complete antigen DAZ-hapten-KLH/BSA was successfully coupled.

The complete antigen DAZ-hapten-KLH was immunized into 10 mice separately, and the titers and inhibitions of the mice sera after five immunizations are shown in **Fig. S2a** and **S2b**. The mouse immunized with 7#-DAZ-hapten-KLH was selected for cell fusion due to its serum titer reaching 81×10^3 and showing a 48% inhibition against DAZ standards.

3.3. Performance of the mAb

3.3.1 Isotype and Affinity

Fig. S2c shows that the mAb 6D9 belongs to the IgG2b subclass and contains a kappa (κ) light chain. In addition, its affinity is 5.52×10^{12} L/mol (**Fig. 3b**). Antibodies with high affinity can be used to develop detection methods that reduce false positive/negative results, while also requiring smaller amounts.

3.3.2 Sensitivity

In the ic-ELISA detection process, it is essential to optimize the buffer solution type to improve the accuracy and reliability of the experiments. In 0.01 M PBS(K^+) containing 10% of DMSO, DMF, MeOH, ACN, EtOH, and a buffer solution with 0% of these additives, the fitted curves yielded IC_{50} values of 0.40, 1.08, 0.77, 4.00, 1.17, and 0.42 ng/mL, respectively (**Fig. S2d**). The IC_{50} at this point was defined as the concentration of the standard corresponding to a B/B0 value of 50%. The smaller the IC_{50} value, the higher the antibody sensitivity. Therefore, we performed the fitting of the standard curve in PBS(K^+) containing 10% DMSO (**Fig. 3a**). The resulting sigmoidal curve was given by the equation $y = 0.000598 + 1.650 / (1 + [x / 0.405]^{0.802})$, with an R^2 of 0.99981, an IC_{50} of 0.4 ng/mL, a limit of detection (LOD) of 0.015 ng/mL, and a linear range of 0.08–2.03 ng/mL. This LOD was defined as the X-value on the standard curve corresponding to the Y-value that was the mean OD_{450nm} value for the no-DAZ concentration minus three times the SD.

The IC_{50} of mAb 1D4 in the ELISA was 0.4 ng/mL, which was lower than the previously reported range of 4–7.5 ng/mL, indicating that the DAZ-hapten is more effective in inducing mAb to enhance recognition capabilities. When comparing hapten structures, we found that the linker arms of haptens 2 and 3 are located at the phosphorothioate group end, whereas the linker arms of hapten 1 and the DAZ-hapten are at the pyrazine ring end, which makes it easier to expose the distal phosphorothioate group, an important organophosphorus group. However, compared to the DAZ-hapten, hapten 1 incorporated a long carbon chain and halogen atoms into its linker arm. Structural comparison analysis revealed that only the DAZ-hapten maintains a high degree of overlap with DAZ in lowest-energy conformations after the introduction of the linker arm (**Fig. 1d**). This also confirmed that the linker arm could cause differences in the performance of the mAb towards small molecule drugs.

3.3.3 Cross-reactivity

With the inhibition of the mAb against DAZ set at 100%, the cross-reactivity and structures of other compounds are shown in **Fig. 3c–3e**. The mAb 6D9 had a cross-reactivity rate of over 10% for PMP-E and CPF, indicating that the mAb 6D9, induced by DAZ hapten with exposed distal phosphorothioate groups, may enhance its

recognition ability for similar compounds [36]. Meanwhile, the cross-reactivity with other structures exposed to organophosphorus / phosphorothioate (methyl) groups was all less than 3%, indicating that a single oxygen analog / methyl group at the distal end of the analogs significantly affected the cross-reactivity rate.

Structurally, DAZ, PMP-E, and CPF all contain the same triazine ring and phosphorothioate group. Among them, DAZ and PMP-E also share the same pyrazine ring, which is identical to the core structure of the DAZ-hapten. In addition, the distal end of the DAZ-hapten is exposed to the phosphorothioate group shared by these three. Importantly, the structural differences between DAZ and PMP-E are mainly replaced by the connecting arms of DAZ hapten, which further exposes more similar functional groups. However, in their three-dimensional lowest-energy conformations, the triazine rings are not coplanar and experience a certain degree of torsion (**Fig. 3d**). This might be one reason why the cross-reactivity rate of mAb 6D9 for PMP-E was only 51%. However, the structures of DAZ and CPF have a relatively better degree of overlap, but they have significant differences on the pyrimidine ring, resulting in a cross-reactivity of only 13%. This result was still higher than the cross-reactivity rates of other hapten-induced antibodies reported in previous studies. Therefore, the cross-reactivity and sensitivity performance of mAb 6D9 is superior to that of other hapten-induced antibodies reported in the literatures [21, 22]. Therefore, the cross-reactivity rate of the mAb 6D9 also somewhat confirms the trend of similarity between the DAZ-hapten and DAZ, PMP-E, CPF.

In addition, although DAX and DAZ differ only by one oxygen atom in their two-dimensional structure, they exhibit significant differences in their three-dimensional lowest-energy conformations (**Fig. 3d**); The distal end of the DAZ-hapten is exposed to phosphorothioate group, which are different from the organophosphorus in DAX. This difference leads to a decrease in the cross-reactivity rate of antibodies against DAX to below 3%. From this, it can be seen that the groups exposed at the distal end of the hapten have a significant impact on the cross reactivity of antibodies. This discovery highlights the effectiveness and reliability of computer simulation analysis in research.

3.4. Establishment of the CG-ICA strip method

3.4.1 Optimization and performance of the CG-ICA strip

The highly sensitive and high-affinity mAb that we prepared was utilized to develop a rapid detection method for food safety testing. For this purpose, we adopted the CG-ICA method and characterized colloidal gold and colloidal gold labeled-mAb conjugate. Colloidal gold, as a stable biological carrier material, exhibits excellent uniformity and optical properties. The successful synthesis of colloidal gold was confirmed by transmission electron microscopy (TEM) and UV–Vis (**Figs. S3a** and **S3b**). After antibody labeling, the UV-Vis spectra revealed a significant redshift and broadening of the absorption peak for the conjugate compared to colloidal gold, and the emergence of a protein absorption peak around 280 nm confirmed the successful conjugation of mAb 6D9 to the colloidal gold. Additionally, dynamic light scattering (DLS) results showed an increase in the hydrodynamic diameter and a change in the *zeta* potential of the conjugate (**Figs. S3c** and **S3d**), further confirming the successful synthesis of the colloidal gold-labeled mAb conjugates. The components and principle

of the test strip are shown in **Fig. S3**. The limitations of CG-ICA testing primarily lie in its sensitivity and specificity. In addition to preparing and selecting materials with high sensitivity, the sensitivity and specificity of CG-ICA detection can also be improved through methodological enhancements [18, 37]. For instance, increasing the reaction rate can be achieved by optimizing the concentration of the reactants and the running buffer.

The reaction rate is directly proportional to the concentration of the reactants; however, excessively high concentrations can lead to non-specific binding, increase background interference, and decrease the detection sensitivity of the method. Therefore, it is essential to determine the optimal concentrations of antigens and antibodies to enhance the sensitivity and accuracy of the detection. The optimization principle for the strip is to select the condition with a T/C value greater than 1.0 and the highest inhibition rate at a DAZ concentration of 0 ng/mL. We chose a labeled mAb dosage of 5 μg, while the T-line was immobilized with 0.08 μg/mL of DAZ-hapten-BSA (**Fig. 4a**). Although the T/C value at a 5 μg labeled mAb dosage is lower than that at 10 μg, using a reduced dosage of antibodies still achieves a satisfactory inhibition rate, thereby decreasing the antibody usage and reducing costs. An appropriate pH value significantly aids in the binding of colloidal gold to proteins. Consequently, we added 30 μL of 0.02 M K_2CO_3 to the colloidal gold-labeled antibody (**Fig. 4b**). The judicious selection and addition of surfactants to the running buffer can enhance the wettability of the strip, maintain the stability of colloidal gold, effectively promote biomolecular reactions, and enhance sensitivity [38, 39]. We optimized the addition of 5% of four surfactants to the basic buffer solution (0.02 M PBS(K^+)), including sucrose; trehalose; mannitol; NaN_3; sodium chloride; potassium chloride; potassium dihydrogen phosphate; and dodecahydrate disodium hydrogen phosphate, to maintain a stable buffer environment and further enhance the stability of the strips. The optimal scenario, with a T/C value greater than 1.0 and the highest inhibition rate of 77.4%, was achieved in the basic buffer solution containing 5% PVP (**Fig. 4c**).

The calibration data used to establish the standard curve in 0.01 M PBS(K^+) are shown in **Fig. S6**. At a DAZ concentration of 0.2 ng/mL, the T-line was slightly lighter than at 0 ng/mL, and it disappeared at 10 ng/mL, thus the visual limit of detection (vLOD) was determined to be 0.2 ng/mL, with a cut-off value of 10 ng/mL. According to calculations, the LOD was 0.15 ng/mL. The vLOD represents the lowest concentration of analyte that can be visually detected on the test strip, while the cut-off value is the signal intensity that determines whether the result displayed on the test strip is positive or negative [40].

3.4.2 Performance of the CG-ICA with real samples

In practice, organic solvents are often required to extract pesticides from biological samples for immunoassays to ensure extraction efficiency. Therefore, based on the optimization results of the previous buffer solution, we compared the effects of different extraction solvents on the DAZ extraction from radish samples for the test strips. **Fig. 4d** shows that all four extraction solutions have strong color development (T/C value greater than 1.0). The highest inhibition rate is observed only when using a 10% DMSO extraction solvent; leading us to select this solvent for the extraction of the target substance from samples. During the actual sample testing, the samples were moderately

diluted before CG-ICA detection to reduce the impact of other components in the matrix on the CG-ICA strips. Therefore, the rationality of the diluent and dilution factor needs to be considered. Accordingly, the actual food sample extraction solvent was diluted two-fold with 0.01 M PBS(K^+) (**Fig. 4e** and **4f**), which allowed for the strip detection to be carried out. Optimization results of CG-ICA visual image are showed in **Fig. S5**.

Standard curves for lake water (0, 0.2, 0.5, 1, 2, 5, and 10 μg/L), radish (0, 0.5, 1, 2, 5, 10, and 20 μg/kg), cucumber and strawberry (0, 1, 2, 5, 10, 20, and 50 μg/kg) at gradient concentrations were established (**Fig. 5**). **Fig. S7** shows the mass spectrometry results identifying these negative samples. The LODs for lake water, radish, cucumber, and strawberry samples determined by the test strips were 0.16 μg/L, 0.33, 0.56, and 1.13 μg/kg, respectively, and the LOQs were 0.30 μg/L, 0.54, 1.14, and 1.57 μg/kg, respectively, with linear ranges of 0.30–10 μg/L, 0.54–20, 1.14–50, and 1.57–50 μg/kg, respectively.

3.5. Verification of the CG-ICA strip

The recovery experiment results shown in **Table 1** verify the accuracy of the above methods. The mean recovery rate was 87.35–106.20%, which was similar to the results of LC–MS, with a coefficient of variation of 1.37–7.60%, confirming the applicability of the rapid screening method for DAZ across various matrices, demonstrating its ability to overcome interference from differently colored matrices. In addition, there was little difference in the recovery rates between vegetables (radish and cucumber) and fruit (strawberry), indicating that the pretreatment and CG-ICA methods could effectively overcome the matrix effect to a certain degree. **Fig. S8** demonstrates that there was no significant alteration in the signal strength of the T/C values of the test strips throughout the 28-day accelerated stability test, indicating that the test strips have sufficient stability [32, 41].

Unknown samples were subjected to three parallel detections using CG-ICA and further validated by LC–MS. The results are shown in **Table 2** and **Fig. S9**. The mean DAZ concentrations in radish and strawberry were 2.7 and 8.8 μg/kg, respectively, while DAZ was not detected in cucumber. This result showed little difference from the LC–MS results. Importantly, due to the advantages of CG-ICA, such as high efficiency and short detection time, it was possible to complete the process “from sample to result” in 5–30 minutes, making it more suitable for rapid on-site detection.

3.6. Method performance comparison

Various detection methods have been proposed for detecting DAZ in food, including instrumental methods, colorimetric methods, and various sensor technologies. In particular, sensor technology has the advantages of fast detection speed and low cost compared to instrumental methods such as GC-MS and HPLC [42-44]. Among these, CG-ICA stands out by overcoming time and space constraints, simplifying pre-processing steps, and making the entire detection process more convenient, faster, and cheaper, making it highly suitable for on-site detection needs. The water sample undergoes direct analysis, and the outcomes are rendered visually within 5 minutes. The CG-ICA strips developed in this study meet China's maximum residue limit requirement for DAZ in radish, cucumber, and strawberry samples, which is 100 μg/kg.

Therefore, the method employed in this study is a design that balances sensitivity and practical applicability. In previous reports, ELISA has been the primary immunoassay method for detecting DAZ [21, 22]. Although ELISA has higher sensitivity, CG-ICA provides better time and operational advantages for rapid on-site detection. Additionally, our developed antibody exhibited higher sensitivity in ELISA tests conducted in a PBS (K^+) (**Table S3**). Based on this mAb, we further developed the CG-ICA method, which represents a novel exploration and application. Compared to ELISA, CG-ICA shows significant advantages in terms of short-term detection, convenience, low cost, and easy interpretation of results, making it more suitable for field testing.

4. Conclusions

A novel hapten, analyzed by computer simulation analysis for structural similarity and matching, has been used to prepare a sensitive mAb and improve their antibody performance. We further developed a rapid, on-site, and visually interpretable CG-ICA strip, which has proven effective for the preliminary screening of DAZ in environmental and food samples. The success of this strategy demonstrates the effectiveness of the innovative design of the DAZ hapten and using computer simulation analysis in assessing hapten suitability for the production of highly sensitive antibodies. It also provides new possibilities and methods for the development of antibodies against other small molecule compounds. We aim to provide a design framework for haptens targeting similar small molecule compounds, thereby opening new possibilities and pathways for the development of antibodies against small molecules. Future research could explore the integration of test strips with other detection technologies to further enhance their sensitivity. This study proposes an innovative hapten design scheme and investigates the practical application of the CG-ICA method using the generated antibodies in environmental and food sample analysis. The proposed approach holds significant promise for advancing the field of rapid, environmental and food safety monitoring.

Disclosure statement

No potential conflict of interest was reported by the authors.

Ethical approval

All animal studies were approved by the Animal Welfare Committee of Jiangnan University and were conducted under strict research procedures and ethical standards, with the audit number JN.No20230415b1801030[121].

Acknowledgements

This work was supported by National Key R&D Program (2024YFF1106102), and National Natural Science Foundation of China (22276076, 22236002, 22306074), the Natural Science Foundation of Jiangsu Province and MOF (BK20230043, BK20212014), and the Fundamental Research Funds for the Central Universities" (JUSRP622032).

References

[1] Y. Wang, R. Xiao, Y. Hu, J. Li, C. Guo, L. Zhang, K. Zhang, M.A. Jorquera, W. Pan, Accumulation and ecological risk assessment of diazinon in surface sediments of Baiyangdian lake and its potential impact on probiotics and pathogens, Environ. Pollut. 357 (2024) 124408.

[2] S. Hajirezaee, A. Mirvaghefi, H. Farahmand, N. Agh, NMR-based metabolomic study on the toxicological effects of pesticide, diazinon on adaptation to sea water by endangered Persian sturgeon, Acipenser persicus fingerlings, Chemosphere 185 (2017) 213-226.

[3] T.M. Mac Loughlin, M.L. Peluso, M.A. Etchegoyen, L.L. Alonso, M.C. de Castro, M.C. Percudani, D.J.G. Marino, Pesticide residues in fruits and vegetables of the argentine domestic market: Occurrence and quality, Food Control 93 (2018) 129-138.

[4] G.L. Wei, C. Wang, W.P. Niu, Q. Huan, T.T. Tian, S.J. Zou, D.Y. Huang, Occurrence and risk assessment of currently used organophosphate pesticides in overlying water and surface sediments in Guangzhou urban waterways, China, Environ. Sci. Pollut. Res. 28(35) (2021) 48194-48206.

[5] G.K. Sidhu, S. Singh, V. Kumar, D.S. Dhanjal, S. Datta, J. Singh, Toxicity, monitoring and biodegradation of organophosphate pesticides: A review, Crit. Rev. Environ. Sci. Technol. 49(13) (2019) 1135-1187.

[6] L.W. Xu, X.X. Xu, X.L. Wu, H. Kuang, C.L. Xu, Sex-Dependent Environmental Health Risk Analysis of Flupyradifurone, Environ. Sci. Technol. 56(3) (2022) 1841-1853.

[7] L.W. Xu, L.L. Guo, Z.X. Wang, X.X. Xu, S. Zhang, X.L. Wu, H. Kuang, C.L. Xu, Profiling and Identification of Biocatalyzed Transformation of Sulfoxaflor In Vivo, Angew. Chem. Int. Ed. 59(37) (2020) 16218-16224.

[8] J. Zhang, X.X. Xu, H. Kuang, C.L. Xu, X.L. Wu, Potential health risk analysis of chlorantraniliprole in vivo, Sci. Bull. 68(22) (2023) 2712-2716.

[9] R. Finger, N. Möhring, The emergence of pesticide-free crop production systems in Europe, Nat. Plants 10(3) (2024) 360-366.

[10] F.H.M. Tang, M. Lenzen, A. McBratney, F. Maggi, Risk of pesticide pollution at the global scale, Nat. Geosci. 14(4) (2021) 206-210.

[11] C.C. Nicholson, J. Knapp, T. Kiljanek, M. Albrecht, M.P. Chauzat, C. Costa, P. de la Rúa, A.M. Klein, M. Mänd, S.G. Potts, O. Schweiger, I. Bottero, E. Cini, J.R. de

Miranda, G. Di Prisco, C. Dominik, S. Hodge, V. Kaunath, A. Knauer, M. Laurent, V. Martínez-López, P. Medrzycki, M.H. Pereira-Peixoto, R. Raimets, J.M. Schwarz, D. Senapathi, G. Tamburini, M.J.F. Brown, J.C. Stout, M. Rundlöf, Pesticide use negatively affects bumble bees across European landscapes, Nature 628(8007) (2024) 355-358.

[12] G. Bellisai, G. Bernasconi, M. Binaglia, L. Carrasco Cabrera, I. Castellan, A.F. Castoldi, A. Chiusolo, K. Chukwubike, F. Crivellente, M. Del Aguila, L. Ferreira, G. Giner Santonja, L. Greco, F. Istace, S. Jarrah, A. Lanzoni, R. Leuschner, I. Mangas, J. Martinez, I. Miron, S. Nave, M. Panzarea, J.M. Parra Morte, R. Pedersen, H. Reich, S. Ruocco, M. Santos, A.P. Scarlato, A. Terron, A. Theobald, M. Tiramani, A. Verani, Targeted review of maximum residue levels (MRLs) for diazinon, EFSA J. 21(11) (2023) 1831-4732.

[13] A. Firoozichahak, A. Rahmani, F. Mehregan, R. Rahimpoor, Sensitive and selective magnetic dispersive microextraction of diazinon from urine samples by molecularly imprinted polymer based on core–shell metal–organic frameworks, J. Chromatogr. B 1207 (2022) 123364.

[14] F. Darvishnejad, J.B. Raoof, M. Ghani, MIL-101 (Cr) @ graphene oxide-reinforced hollow fiber solid-phase microextraction coupled with high-performance liquid chromatography to determine diazinon and chlorpyrifos in tomato, cucumber and agricultural water, Anal. Chim. Acta 1140 (2020) 99-110.

[15] Y. Wang, M. Li, Z. Wang, J. Xu, J. Zhao, Z.-D. Gao, Y.-Y. Song, Photothermal effect-enhanced peroxidase-like performance for sensitive detection of organophosphorus pesticides on a visual test strip, Chem. Eng. J. 476 (2023) 146329.

[16] X. Zhang, Z. Wang, X. Huang, Q. Huang, Y. Wen, B. Li, M. Holmes, J. Shi, X. Zou, Uniform stain pattern of robust MOF-mediated probe for flexible paper-based colorimetric sensing toward environmental pesticide exposure, Chem. Eng. J. 451 (2023) 138928.

[17] T. Qin, X. Zhao, C. Song, T. Lv, S. Chen, Z. Xun, Z. Xu, Z. Zhang, H. Xu, C. Zhao, B. Liu, X. Peng, A ratiometric supramolecular fluorescent probe for on-site determination of cyfluthrin in real food samples, Chem. Eng. J. 451 (2023) 139022.

[18] Y. Liu, L. Zhan, Z. Qin, J. Sackrison, J.C. Bischof, Ultrasensitive and Highly Specific Lateral Flow Assays for Point-of-Care Diagnosis, ACS Nano 15(3) (2021) 3593-3611.

[19] Z. Li, Q. Cui, Q. Li, C. Luo, M. Chen, B. Feng, H. Li, T. Bu, Y. Mao, M. Dang, X. Huang, L. Song, D. Peng, X. Zhang, Preparation of ultra-sensitive anti-carbendazim

antibodies based on new haptens and their application in lateral flow immunoassay, Sensors Actuators B: Chem. 412 (2024) 135751.

[20] W. Wu, C. Li, D. Liu, J. Ji, J. Zhu, H. Lu, B. Fu, Y. Ma, Ultrasensitive antibody production strategy based on hapten property for simultaneous immunoassay, Food Chem. 395 (2022) 133565.

[21] E.M. Brun, M. Garces-Garcia, E. Escuin, S. Morais, R. Puchades, A. Maquieira, Assessment of novel diazinon immunoassays for water analysis, Environ. Sci. Technol. 38(4) (2004) 1115-23.

[22] E.K. Lee, Y.J. Kim, W.C. Park, T. Chung, Y.T. Lee, Monoclonal antibody-based enzyme-linked immunosorbent assays for the detection of the organophosphorus insecticide diazinon, Anal. Chim. Acta 530(1) (2005) 143-153.

[23] J. Fei, J. Jiang, Y. Bai, W. Wu, X. Zhao, W. Yu, K. Wen, X. Yu, J. Shen, Z. Wang, A Proof-of-Concept Sandwich Enzyme-Linked Immunoassay Development for Small Molecules, Anal. Chem. 95(39) (2023) 14665-14674.

[24] Y. Zhang, W. Wu, Q. Li, P. Zhou, K. Wen, J. Shen, Z. Wang, The hapten rigidity improves antibody performances in immunoassay for rifamycins: Immunovalidation and molecular mechanism, J. Hazard. Mater. 469 (2024) 133977.

[25] S. Yu, G. Zhang, L.M. Hu, H.Y. Ji, J.W. Chen, J. Peng, W.H. Lai, Strong light-trapping probes with high antibody activity for sensitive detecting FB1 by "turn-on" lateral flow immunoassay, Chem. Eng. J. 496 (2024) 154032.

[26] J. Li, L. Jiang, Y. Shu, S. Song, L. Xu, H. Kuang, C. Xu, L. Guo, Quantitative immunochromatographic assay for rapid and cost-effective on-site detection of benzo[a]pyrene in oilfield chemicals, J. Hazard. Mater. 469 (2024) 134100.

[27] L. Zeng, X. Xu, L. Guo, Z. Wang, H. Ding, S. Song, L. Xu, H. Kuang, L. Liu, C. Xu, An immunochromatographic sensor for ultrasensitive and direct detection of histamine in fish, J. Hazard. Mater. 419 (2021) 126533.

[28] G. Fu, Y. Duan, W. Yi, S. Zhang, W. Liang, H. Li, H. Yan, B. Wu, S. Fu, J. Zhang, G. Zhang, G. Wang, Y. Liu, S. Xu, A rapid and reliable immunochromatographic strip for detecting paraquat poinsoning in domestic water and real human samples, Environ. Pollut. 315 (2022) 120324.

[29] H.H. Wu, L.L. Guo, X.X. Xu, J. Zou, H. Kuang, C.L. Xu, X.L. Wu, On-site rapid detection of perfluorooctanoic acid by visual immunochromatographic strip biosensor in domestic water and real human samples, Environ. Pollut. 348 (2024) 123776.

[30] Q. Lu, X. Xu, A. Qu, L. Liu, Y. Li, M. Sun, C. Xu, H. Kuang, A multi-colloidal gold immunochromatography assay for rapid and simultaneous detection of 13 herbicides, Nano Res. 17(9) (2024) 8368-8376.

[31] Y. Zha, Y. Li, J. Zhou, X. Liu, K.S. Park, Y. Zhou, Dual-Mode Fluorescent/Intelligent Lateral Flow Immunoassay Based on Machine Learning Algorithm for Ultrasensitive Analysis of Chloroacetamide Herbicides, Anal. Chem. 96(29) (2024) 12197-12204.

[32] D. Wang, J. Wang, D. Liu, J. He, M. Wang, H. Huang, G. Nie, H. Ding, X. Yan, Rapid and sensitive detection of Epstein-Barr virus antibodies in nasopharyngeal carcinoma by chemiluminescence strips based on iron-porphyrin single atom nanozyme, Nano Res. 17(3) (2023) 1827-1836.

[33] A. Geistanger, K. Braese, R. Laubender, Automated data analytics workflow for stability experiments based on regression analysis, Mass Spectrom Adv 24 (2022) 5-14.

[34] Y. Zhu, Y. Zhang, D. Zeng, H. Chen, Y. Wang, J. Yang, H. Wang, Z. Xu, Y. Sun, Y. Tian, Y. Shen, Designing a size exclusion-based hapten and the development of a quantitative and visual time-resolved fluorescence immunochromatography assay strip for detecting dimethomorph and flumorph in a group-specific manner, Food Chem. 450 (2024) 139372.

[35] H.H. Wu, A.H. Wu, L.Q. Liu, H. Kuang, M.Z. Sun, C.L. Xu, X.X. Xu, Computerized analysis of haptens for the ultrasensitive and specific detection of Pyriftalid, J. Hazard. Mater. 474 (2024) 134705.

[36] Z. Li, J. Wang, Y. Wang, Q. Li, X. Chen, Y. Wang, H. Tian, Y. Mao, L. Song, X. Huang, Z. Wang, X. Zhang, Development of a Lateral Flow Immunoassay Based on a Highly Specific Monoclonal Antibody To Detect 4-Methylaminoantipyrine, J. Agric. Food Chem. 71(28) (2023) 10841-10849.

[37] Z. Wang, Y. Guo, Y. Xianyu, Applications of self-assembly strategies in immunoassays: A review, Coord. Chem. Rev. 478 (2023) 214974.

[38] J. Li, H. Wang, L. Wang, D. Yu, X. Zhang, Stabilization effects of saccharides in protein formulations: A review of sucrose, trehalose, cyclodextrins and dextrans, Eur. J. Pharm. Sci. 192 (2024) 106625.

[39] W.-C. Luo, A. O'Reilly Beringhs, R. Kim, W. Zhang, S.M. Patel, R.H. Bogner, X. Lu, Impact of formulation on the quality and stability of freeze-dried nanoparticles, Eur. J. Pharm. Biopharm. 169 (2021) 256-267.

[40] X. Huang, G. Zhang, Z. Fang, X. Lai, X. Xiao, J. Peng, W. Lai, Nanomodification engineering facilitated efficient fluorescence quenchers for developing sensitive lateral flow immunoassay, Chem. Eng. J. 492 (2024) 152136.

[41] H. Fan, R. Li, Y. Chen, Q. Da, C. Xiong, Y. Zhang, Z. Qin, G.L. Liu, L. Huang, Sample-to-answer point-of-care testing platform for quantitative detection of small molecules in blood using a smartphone-and microfluidic-based nanoplasmonic biosensor, Chem. Eng. J. 501 (2024) 157495.

[42] S. Khaledian, A. Noroozi-Aghideh, D. Kahrizi, S. Moradi, M. Abdoli, A.H. Ghasemalian, M.F. Heidari, Rapid detection of diazinon as an organophosphorus poison in real samples using fluorescence carbon dots, Inorg. Chem. Commun. 130 (2021) 108676.

[43] P. Wang, H. Li, M.M. Hassan, Z. Guo, Z.-Z. Zhang, Q. Chen, Fabricating an Acetylcholinesterase Modulated UCNPs-Cu2+ Fluorescence Biosensor for Ultrasensitive Detection of Organophosphorus Pesticides-Diazinon in Food, J. Agric. Food Chem. 67(14) (2019) 4071-4079.

[44] J. Tan, B. Peng, L. Tang, C. Feng, J. Wang, J. Yu, X. Ouyang, X. Zhu, Enhanced photoelectric conversion efficiency: A novel h-BN based self-powered photoelectrochemical aptasensor for ultrasensitive detection of diazinon, Biosens. Bioelectron. 142 (2019) 111546.

Captions

Fig. 1. (a) The structure of DAZ and partial analogs. (b) Two-dimensional structures of different haptens. (c) Similarity between different haptens and analogs. (d) Three-dimensional structures between different haptens and DAZ. (e) Partial atomic charges between DAZ-hapten and DAZ. (f) ESP of DAZ and DAZ-hapten.

Fig. 2. (a) The *de novo* synthesis scheme of DAZ-hapten. (b) Structures of DAZ, DAZ-hapten and complete antigen. (c) Liquid chromatogram and purity of DAZ-hapten. (d) Mass spectrometry characterization of DAZ-hapten. (e) Nuclear magnetic resonance spectroscopy spectrum of DAZ-hapten.

Fig. 3. Characteristics of the mAb 6D9 and structures of analytes and analogs. (a) Final standard curve. (b) Curve of affinity. (c) Cross-reactivity (1. diazinon (DAZ), 2. pirimiphos-ethyl (PMP-E), 3. chlorpyrifos (CPF), 4. diazoxon (DAX), 5. triazophos (TZP), 6. quinalphos (QNP), 7. pirimiphos-methyl (PMP-M), 8. parathion (PTN), 9. chlorpyrifos-methyl (CPF-M), 10. fenthion, 11. parathion-methyl (PTN-M), 12. fenitrothion (FNT), 13. phoxim, 14. etrimfos). (d) Three-dimensional structural comparison of DAZ with PMP-M, DSP, and DAX. (e) The structure of partial analogs.

Fig. 4. Optimization of the CG-ICA method. (a) Concentration of T-line and the amount of mAb labeled (in a 10 mL colloidal gold solution). (b) The amount of K_2CO_3 used. (The color development of the actual strips was lighter at lower concentrations, thus both T/C values and T values were compared). (c) Resuspension solution. (d) Extraction solvent of food samples. (e) Dilution fold of food samples. (f) Diluent solution of food samples.

Fig. 5. Visual images and corresponding standard curves for DAZ detection in lake water, radish, cucumber, and strawberry samples using CG-ICA strips.

Table 1

Examined the spiked-DAZ in water and food specimens using the CG-ICA method, and verified by LC–MS (n = 3).

Table 2

Comparation of CG-ICA and LC–MS for DAZ in unknown samples (n = 3).

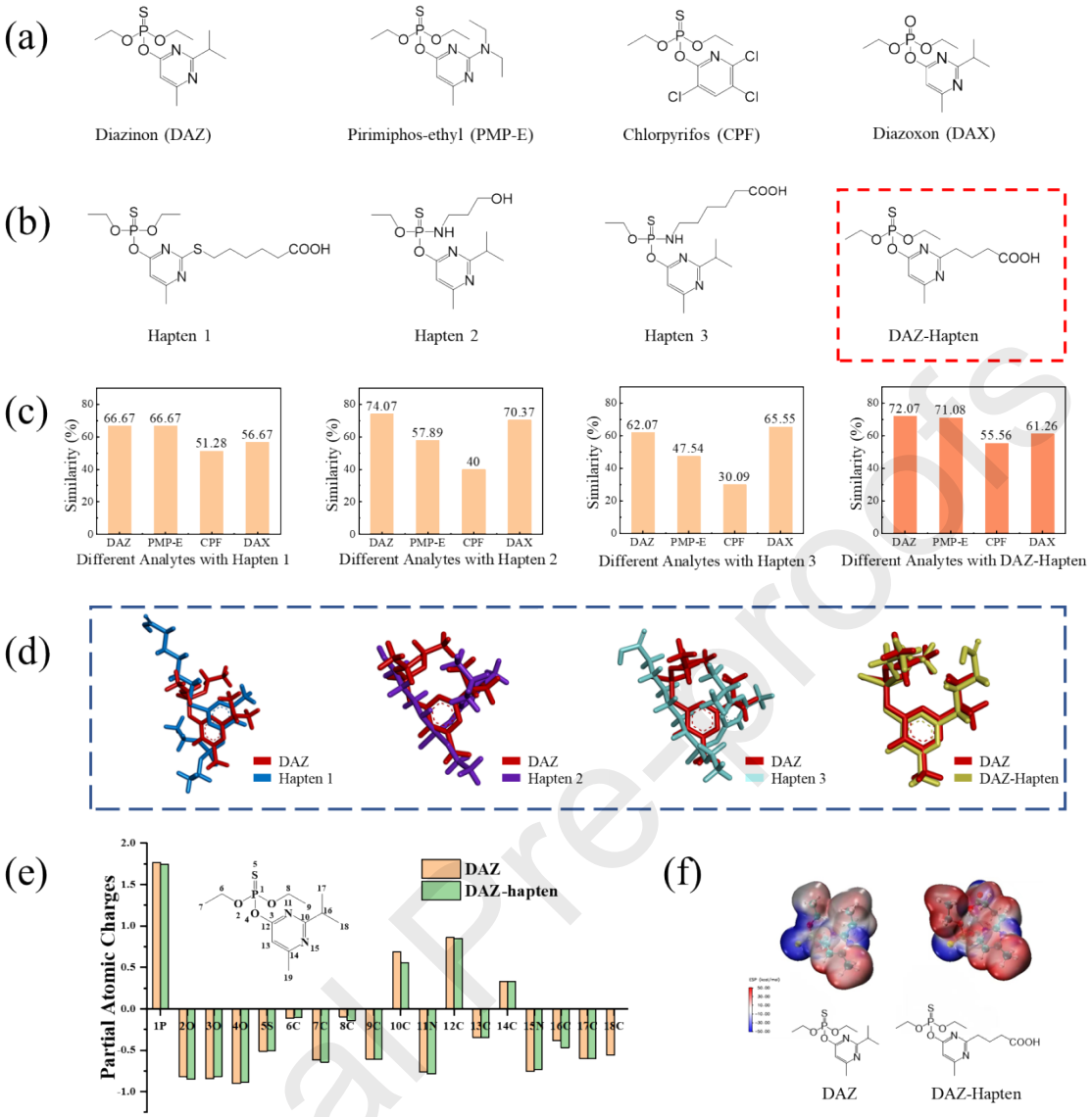

Fig. 1. (a) The structure of DAZ and partial analogs. (b) Two-dimensional structures of different haptens. (c) Similarity between different haptens and analogs. (d) Three-dimensional structures between different haptens and DAZ. (e) Partial atomic charges between DAZ-hapten and DAZ. (f) ESP of DAZ and DAZ-hapten.

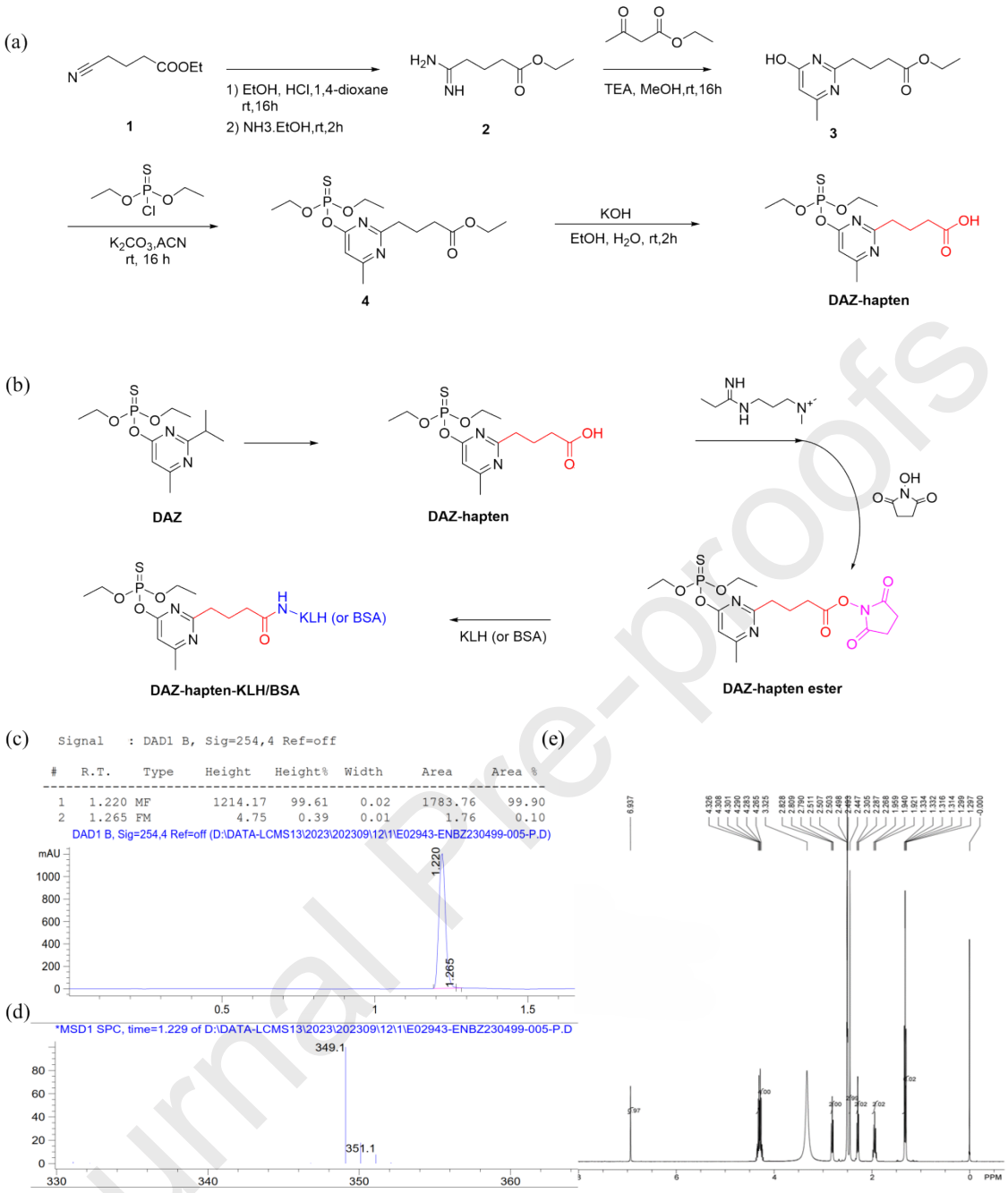

Fig. 2. (a) The *de novo* synthesis scheme of DAZ-hapten. (b) Structures of DAZ, DAZ-hapten and complete antigen. (c) Liquid chromatogram and purity of DAZ-hapten. (d) Mass spectrometry characterization of DAZ-hapten. (e) Nuclear magnetic resonance spectroscopy spectrum of DAZ-hapten.

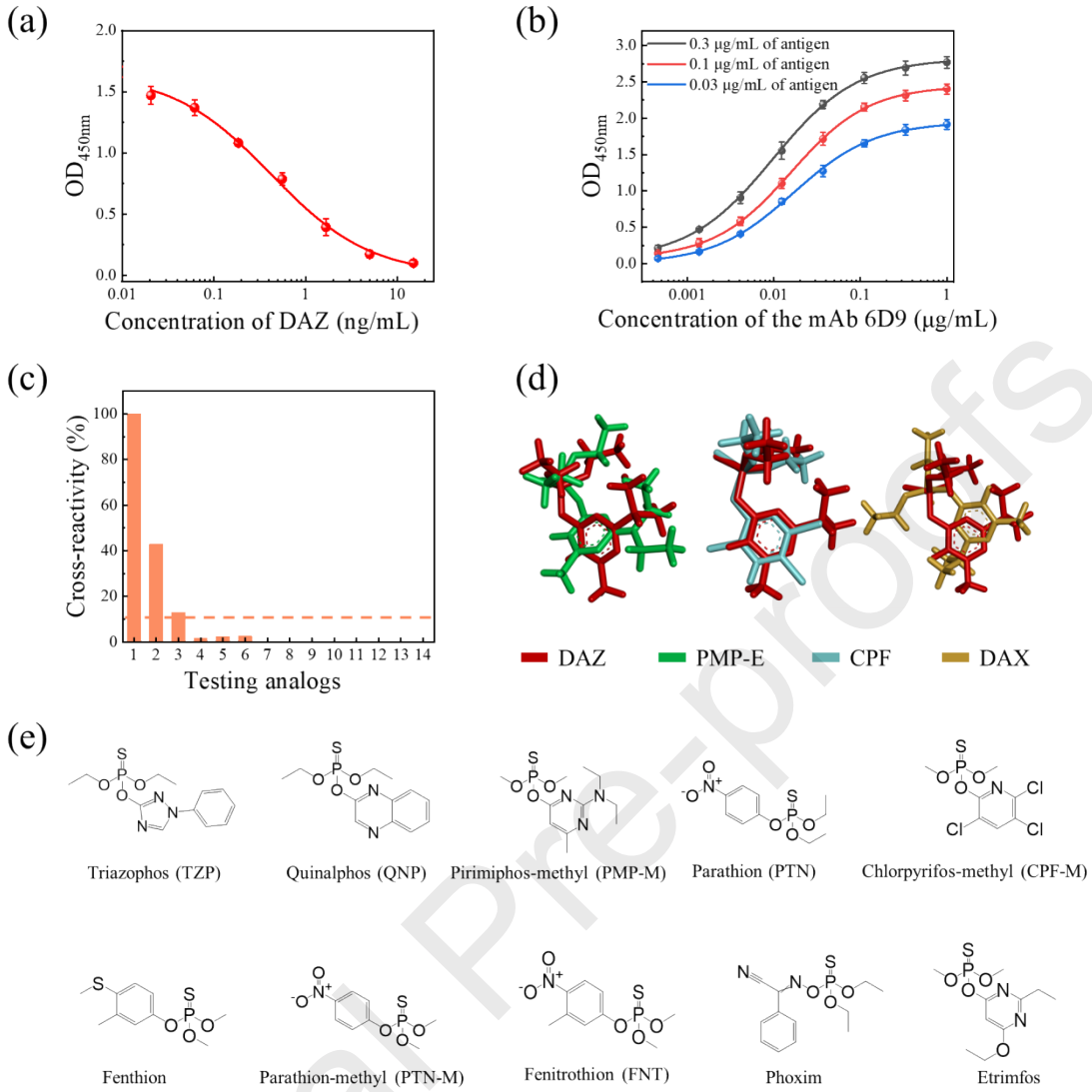

Fig. 3. Characteristics of the mAb 6D9 and structures of analytes and analogs. (a) Final standard curve. (b) Curve of affinity. (c) Cross-reactivity (1. diazinon (DAZ), 2. pirimiphos-ethyl (PMP-E), 3. chlorpyrifos (CPF), 4. diazoxon (DAX), 5. triazophos (TZP), 6. quinalphos (QNP), 7. pirimiphos-methyl (PMP-M), 8. parathion (PTN), 9. chlorpyrifos-methyl (CPF-M), 10. fenthion, 11. parathion-methyl (PTN-M), 12. fenitrothion (FNT), 13. phoxim, 14. etrimfos). (d) Three-dimensional structural comparison of DAZ with PMP-M, DSP, and DAX. (e) The structure of partial analogs.

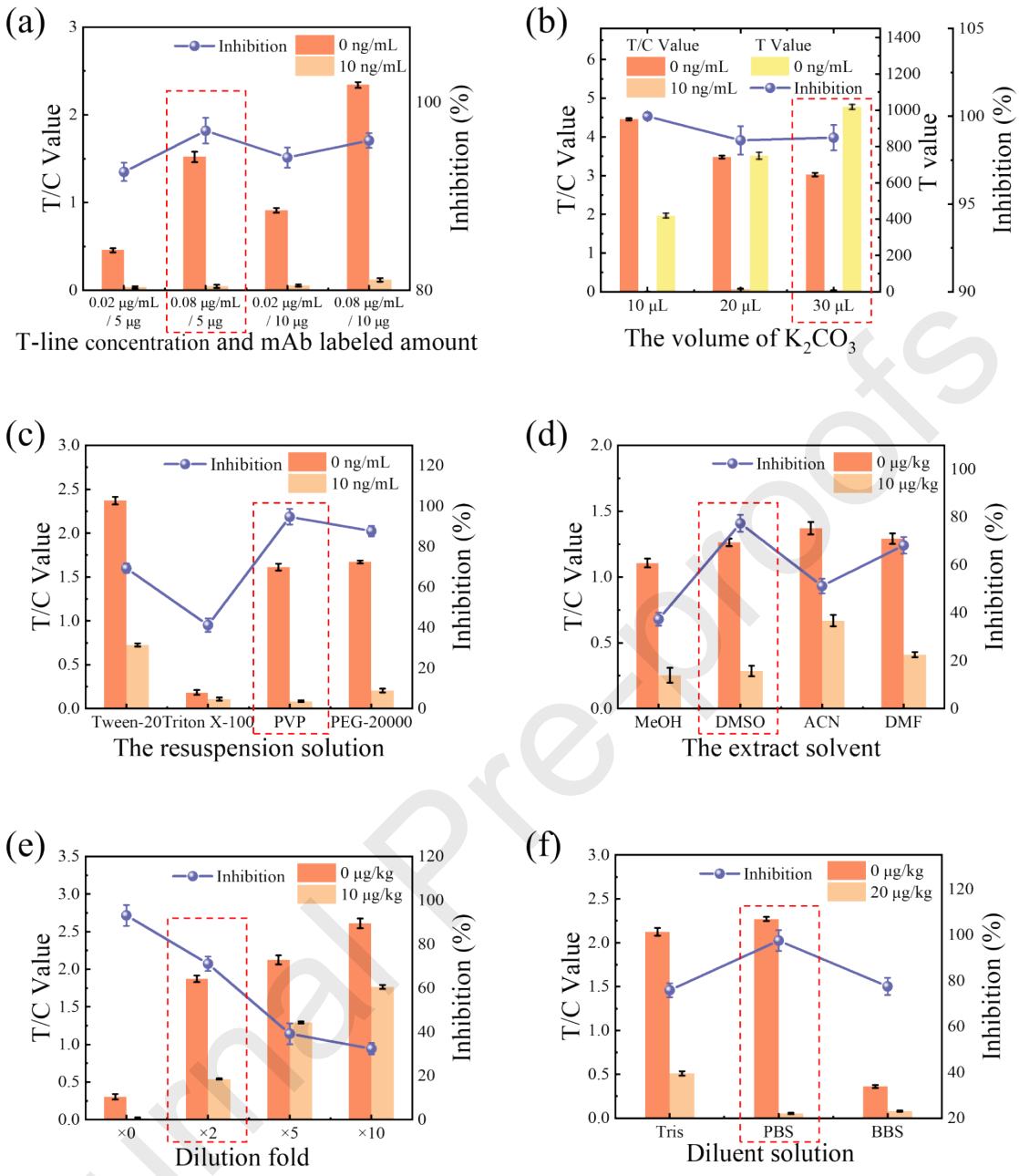

Fig. 4. Optimization of the CG-ICA method. (a) Concentration of T-line and the amount of mAb labeled (in a 10 mL colloidal gold solution). (b) The amount of K_2CO_3 used. (The color development of the actual strips was lighter at lower concentrations, thus both T/C values and T values were compared). (c) Resuspension solution. (d) Extraction solvent of food samples (10% organic solvent equivalent). (e) Dilution fold of food samples. (f) Diluent solution of food samples.

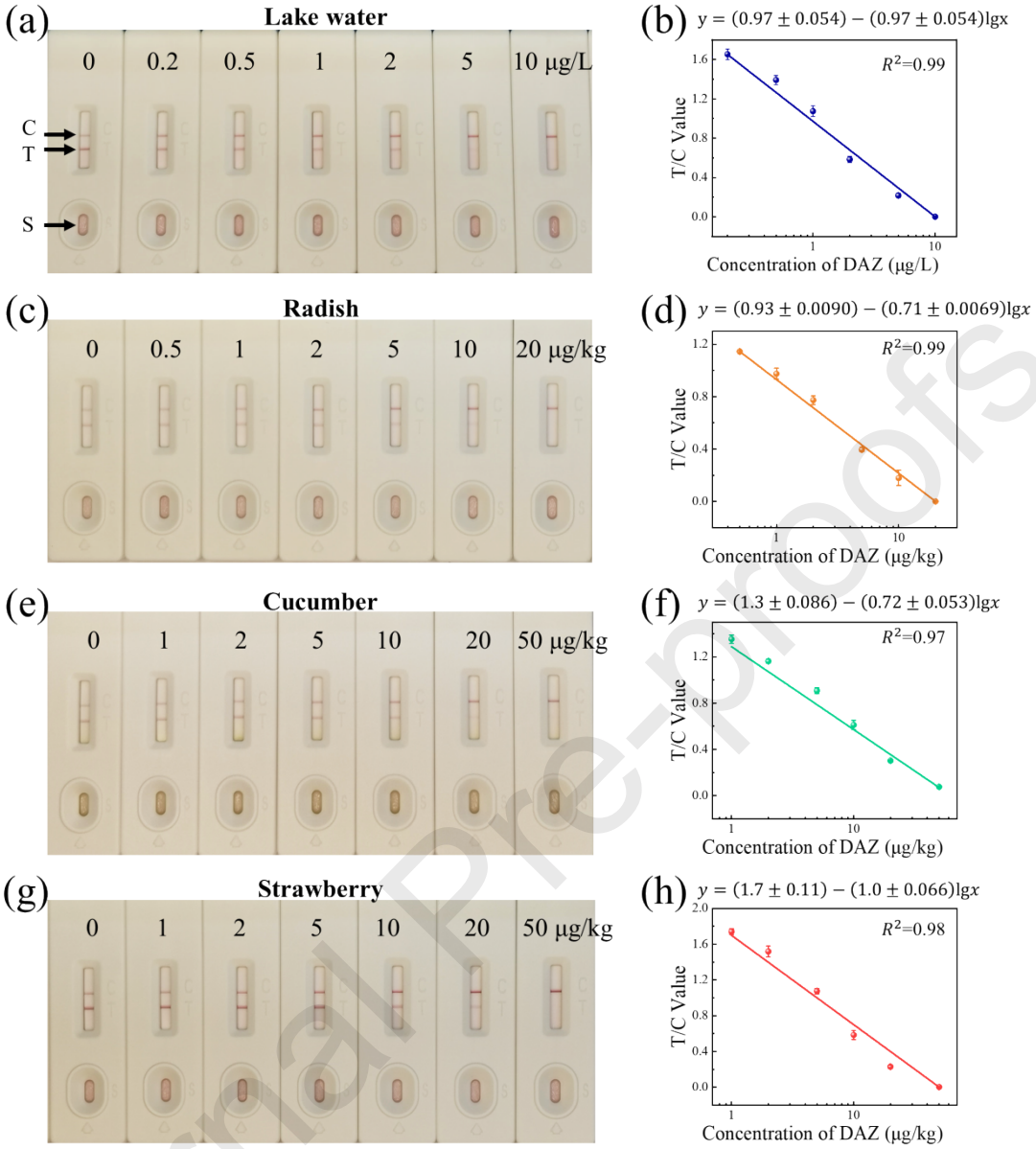

Fig. 5. Visual images and corresponding standard curves for DAZ detection in lake water, radish, cucumber, and strawberry samples using CG-ICA strips.

Table 1

Examined the spiked-DAZ in lake water and food specimens using the CG-ICA method, and verified by LC–MS (n = 3).

Sample	Spiked level (μg/kg)	CG-ICA strip				LC–MS		
		Quantitative detection			Qualitative results	Detected mean (μg/kg) ± SD	Recovery (%) ± SD	CV (%)
		Detected mean (μg/kg) ± SD	Recovery (%) ± SD	CV (%)				
Lake water	0	ND [a]	NC[b]	NC	- [c]	ND	NC	NC
	1	0.98 ± 0.07	98.00 ± 6.64	6.78	++ [d]	0.91 ± 0.03	91.10 ± 3.42	3.75
	5	5.31 ± 0.29	106.20 ± 5.73	5.39	+++	5.02 ± 0.27	100.37 ± 5.38	5.36
Radish	0	ND	NC	NC	-	ND	NC	NC
	1	0.87 ± 0.07	87.35 ± 6.64	7.60	++	0.90 ± 0.03	90.31 ± 3.42	3.78
	5	4.78 ± 0.36	95.60 ± 7.26	7.59	+++	4.86 ± 0.37	97.28 ± 7.38	7.58
Cucumber	0	ND	NC	NC	-	ND	NC	NC
	2	1.91 ± 0.05	95.50 ± 2.69	2.81	++	1.94 ± 0.05	97.22 ± 2.61	2.69
	15	14.87 ± 0.20	99.13 ± 1.36	1.37	+++	14.69 ± 0.55	97.92 ± 3.70	3.77
Strawberry	0	ND	NC	NC	-	ND	NC	NC
	2	1.84 ± 0.10	91.89 ± 4.83	5.25	++	1.98 ± 0.08	99.04 ± 4.16	4.20

	15	14.20 ± 0.87		94.67± 5.78	6.11	±±±	14.33 ± 0.75		95.53 ± 4.99	5.23

[a] ND, not detectable;

[b] NC, not calculated;

[c] -, negative results;

[d] ±, weak positive results of visual inspection, measured concentration of DAZ was 0.2–10 μg/L in lake water, 0.5–20 μg/kg in radish, 1–50 μg/kg in cucumber and strawberry.

Table 2

Comparation of CG-ICA and LC–MS for DAZ in unknown samples (n = 3).

Samples	CG-ICA (μg/kg)	LC–MS (μg/kg)	Relative accuracy (%)
Sample 1	3	2.77	92%
Sample 2	ND	ND	100%
Sample 3	9.5	8.80	93%

Highlights

- On-site method developed for monitoring Diazinon pesticide in environmental and food samples.
- Novel Diazinon haptens were proposed via computationally modeled to evaluate their functional similarity.
- A visual CG-ICA method was developed capable of detecting Diazinon within 10 minutes.
- The CG-ICA detection results were in agreement with the LC-MS detection results.